Proceedings of the ASME 2010 3rd Joint US-European Fluids Engineering Summer Meeting and 8th International Conference on Nanochannels, Microchannels, and Minichannels
FEDSM-ICNMM2010
August 1-5, 2010, Montreal, Canada

FEDSM-ICNMM2010-30946

ANALYSIS OF DOOR MIRROR AEROACOUSTIC SOURCE USING EXTENDED PROPER ORTHOGONAL DECOMPOSITION

Abbas Hekmati*
Advanced Automotive Technologies Department
RENAULT
Institut Jean Le Rond d'Alembert
University of Pierre et Marie Curie-Paris 6
FR TCR AVA 163 - 1 av. du golf 78288 Guyancourt-France
Email: abbas.hekmati@renault.com

Denis Ricot
Advanced Automotive Technologies Department
RENAULT
FR TCR AVA 163 - 1 av. du golf 78288 Guyancourt-France
denis.ricot@renault.com

Philippe Druault
Institut Jean Le Rond d'Alembert
University of Pierre et Marie Curie-Paris 6
75252 Paris cedex 5-France
philippe.druault@upmc.fr

Keywords: Aeroacoustics, Extended Proper Orthogonal Decomposition

ABSTRACT

Based on a 3D simulation of the air flow around a vehicle, the Extended Proper Orthogonal Decomposition (EPOD) is employed in order to identify the existing relation between aerodynamic events around the door mirror (Ω domain) and the near acoustic pressure field (S domain). The aerodynamic pressure field on a 2D plan of Ω is decomposed using a classical formulation of POD. These modes are then sorted according to their correlation to the acoustic pressure field. The modes for which this correlation value is higher than a given threshold are selected. The proposed threshold determination is detailed. The selected modes are then employed in an EPOD procedure in order to determine their contribution to the acoustic pressure field. The aerodynamic pressure field reconstructed by these selected modes has a good correlation with the acoustic pressure field. This correlation is higher than the correlation between the aerodynamic pressure field reconstructed by the most energetic modes and the acoustic pressure field.

INTRODUCTION

The modern automotive industry has achieved significant progresses in passenger acoustic comfort. Today the contribution of the aerodynamically generated noises is not negligible. In such industrial application the turbulent flows are present and the analysis of noise generation mechanisms occurring in turbulent flows has to be properly investigated. Such analyses are becoming of primary interest for many flow applications related to noise control flow strategies.

The recent progress in numerical simulation provides reliable data in those zones where the sound generation is concentrated. Moreover in some cases the propagation of the acoustic pressure fluctuations can be correctly modeled in the same simulation. For instance, the Direct Noise Calculation of low Mach

*Address all correspondence to this author.

number flows can be efficiently performed by the Lattice Boltzmann Method based solvers [1, 2]. The access to flow variables in the sound generation region and the associated acoustic field provides the possibility of checking the theoretical models and investigating the phenomena involved in the sound production. The last investigation can be done using causality methods [3–6]. Such methods are based on the correlation of the acoustic pressure field with either the flow quantities or a combination of these quantities representing a theoretical definition of acoustic sources. For instance, Bogey and Bailly [3] used space-time pressure/velocity correlations to investigate the relation between the emitted acoustic pressure and flow quantities. Their analysis is mostly aimed at correlating the acoustic pressure and turbulent broadband signals. Other possible statistical analysis can be performed using Quadratic Stochastic Estimation coupled to modal decompositions in order to bridge between aerodynamic events and sound generation [4]. Also, Freund [7] has developed some models to work out the contribution of the jet flow to the acoustic field. In his study, the Fourier transform in time and space (along the axial coordinate) domains is applied to the Lighthill's theoretical expression of acoustic source [8]. Then, this signal is filtered in order to identify and separate components capable of radiating sound to the far field. Indeed the turbulent events that generate the acoustic fluctuations can be best represented by the Lighthill's source term, but they may be identified by other turbulent quantities [3]. For instance, the pressure is related to the velocity field through the Poisson equation. The source term of the Poisson equation has the same form as the source term of Lighthill analogy. Regarding to these equations the pressure field is a good variable to describe the volumetric source field. In particular, the non-linear velocity terms are naturally embedded in the pressure field. In this study we choose the aerodynamic fluctuating pressure field in the source region (Ω) to study the turbulent events responsible of the acoustic pressure generation. The relation between source events and the acoustic field is investigated by the Extended Proper Orthogonal Decomposition (EPOD) [9]. In the first step this spatio-temporal aerodynamic pressure field is decomposed by using Proper Orthogonal Decomposition. Then, the correlation of these modes with acoustic pressure is investigated with an EPOD procedure.

A three-dimensional numerical simulation of external flow around a real vehicle model is performed. In order to simplify the analysis of the noise generating aerodynamic mechanisms, the acoustic pressure is considered in the exterior where the turbulent activities are absent. Obviously many parts participate in aeroacoustic noise generation, but here we chose to study only the generated noise related to the door mirrors. This region, called source region in the following, is chosen firstly because it contains high turbulent interactions, secondly because it is situated in the near neighborhood of windows and could contribute efficiently to the interior noise.

Computational set-up

3D external flow around a vehicle is simulated by PowerFLOW, which is based on Lattice Boltzmann Method (LBM). The LBM is a powerful technique for the computational modeling of a wide variety of complex flow problems [10]. In particular, the LBM shows a high performance for Direct Noise Calculations (DNC) in low Mach numbers [11–16].

The acoustic capabilities of PowerFLOW have been investigated using simple simulation cases such as the acoustic pulse propagation [11, 17], the computation of acoustic resonances of some cavities [11, 17] and the computation of the acoustic reflection coefficient of an open-end duct termination [1].

A similar application of the DNC of the air flow around a vehicle has been already performed by Adam *et al.* [2]. In their study a beamforming algorithm is used in order to determine the contribution of aerodynamic events around the door mirrors to the acoustic field. The acoustic pressure field is probed by in a set of points located at the nearest distance of the vehicle where the turbulent activities are absent. The obtained acoustic pressure signals are then delayed with respect to their distance to the focusing point and summed in order to determine the contribution of turbulent activities in the focusing point to the acoustic field. The obtained results show a good correlation with the experimental ones for frequencies up to 2000 Hz. The volume mesh used in the present work is coarser than the mesh used by Adam *et al.* [2] and it would be expected to obtain a lower frequency limit.

The air flow is simulated around the whole vehicle at 120 km/h. Figure 1 shows an instantaneous velocity magnitude field. Based on previous studies, for a better consideration of aeroacoustic sources, a higher resolution is selected for mesh where the turbulent activities are important. In particular, the finest mesh resolution, 2.4 mm is considered around the door mirror as in this study we are interested in the generated noise associated with the turbulent activities in this region. The resolution is reasonably decreased in other zones to maintain the simulation size affordable while paying attention to not to damage the propagation of the acoustic pressure fluctuations. The simulation contains a total number of 6.9×10^7 mesh points and 1.5×10^5 converged time-steps. Each time step correspond to a physical time of 4.171×10^{-6} s providing a total simulated time of 0.62 s.

Figure 2 shows the wireframe of the volume surrounding the left door mirror in which spatio-temporal pressure field is stored every 4 time-steps. The available data is sub-sampled (every 16 time-steps) for all the following analyses. A total number of 30 probes linearly aligned in y direction (perpendicular to the side window) starting from 0.35 m of the side window and spaced by 0.05 m are considered to detect the acoustic pressure.

A phase relation analysis is successively carried out on each pair of probes in order to check that the pressure signals at these probes are purely acoustic pressure signals. For this purpose, the Fourier transformation is applied to the stored temporal signals.

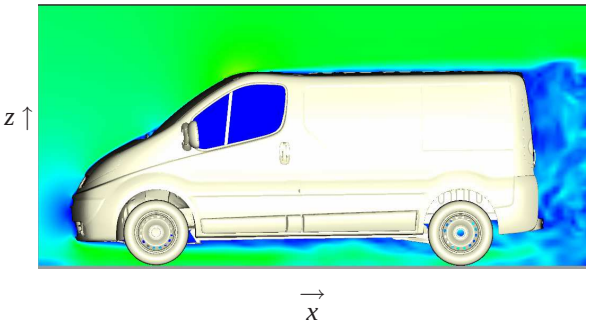

Figure 1. Instantaneous velocity magnitude field. The entry velocity is fixed at 120 km/s in x direction.

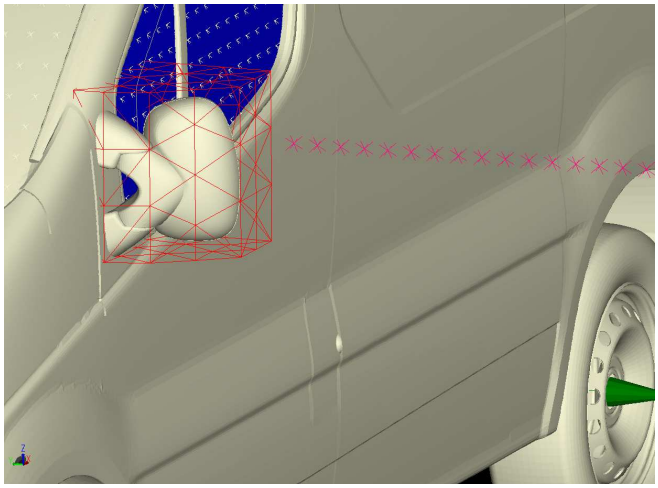

Figure 2. Aerodynamic pressure field is assessed in red box surrounding the door mirror shown in wireframe. Thirty probes are considered to detect the acoustic pressure fluctuations shown in pink crosses.

A total number of 6 FFT blocks containing 3112 independent temporal samples with an overlap of 50% are averaged. A Hamming window is used. Each block represents 0.2 s of physical time. The relative phase between two successive points for the corresponding FFT blocks is calculated and averaged:

$$\left\langle P_n^{(l)}(\mathbf{x}_n,f)P_m^{*(l)}(\mathbf{x}_m,f)\right\rangle = \left\langle p_n^{(l)}e^{i\varphi_n^{(l)}}\,p_m^{(l)}e^{-i\varphi_m^{(l)}}\right\rangle,$$
$$\tilde{\Delta\varphi}_{nm} = \left\langle \varphi_n^{(l)} - \varphi_m^{(l)}\right\rangle,$$

where $\langle\ \rangle$ represents the mean value calculated on the FFT blocks that are indicated by l. This value is then compared by relative phase associated with an acoustic plane wave propagating in y direction, the direction of the alignment of probes:

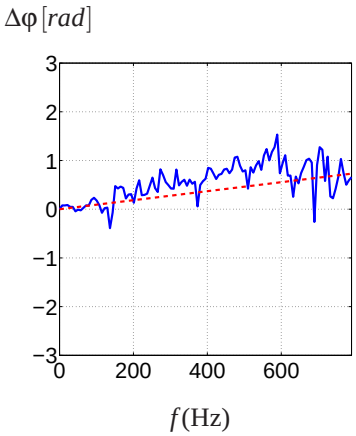

Figure 3. Relative phase between two points situated at 0.55 cm and 0.6 cm of the left door mirror: (—) measurement supplied by the simulation, (- - -) theoretical value for the propagation velocity of 340 m/s.

$$\Delta\varphi_{nm} = k_y(|\mathbf{x}_n - \mathbf{x}_m|) = \frac{2\pi f}{c}(|\mathbf{x}_n - \mathbf{x}_m|) \qquad (1)$$

This procedure allows the detection of the nearest probe to the vehicle which is out of turbulent region of the flow. Figure 3 shows the phase relation between probes situated successively in 0.55 m and 0.6 m of the left side window. On the same figure the theoretical phase is drawn for a propagation velocity of c=340 m/s. The relative phase between these two points confirms an acoustic wave propagation until 800 Hz. For higher frequencies the relative phase is too much noisy for any conclusion about the nature of the signals.

As all the following analyses are carried out in temporal domain, all temporal data is filtered for frequencies higher than simulation's cut off frequency, $f_c = 1500$ Hz. This filtering is mainly done to remove the spurious high frequency components and to improve the accuracy of temporal correlations.

In this work the detection of the aerodynamic events around the door mirror that contribute to the acoustic field is not carried out on the whole volume shown in figure 2. The analyses are restricted to a 2D plan shown in figure 4. This plan is parallel to xy plan and chosen in the middle of the two mounting bases of the door mirror. In the following Ω refers to this plane and the space variable in Ω is indicated by $\mathbf{x}_1 = (x_1, y_1, z_1)$. The spatial domain of the acoustic pressure field is indicated by S and $\mathbf{x}_2 = (x_2, y_2, z_2)$ is the space variable in S.

Followed methodology and mathematical tools

Considering the fluctuating pressure field $p(\mathbf{x}_1, t)$, the Proper Orthogonal Decomposition provides a set of mutually or-

(a)

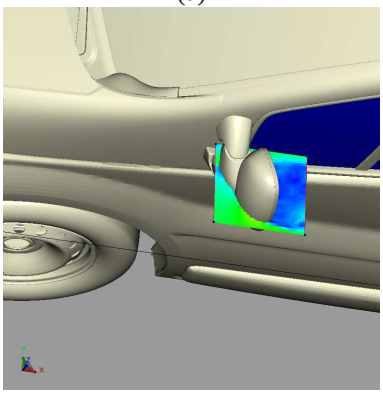

(b)

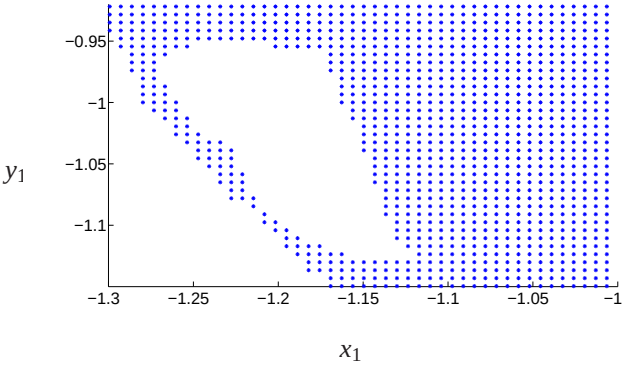

Figure 4. (a) 2D plan used for aerodynamic pressure assessing. (b) available mesh points on this plan.

thogonal and deterministic functions acquiring the largest mean square projection of $p(\mathbf{x}_1,t)$ [18]. These functions are the solutions of the following Fredholm equation [19]:

$$\int_\Omega R_{pp}(\mathbf{x}_1,\mathbf{x}_1')\phi^{(n)}(\mathbf{x}_1')d\mathbf{x}_1' = \lambda^{(n)}\phi^{(n)}(\mathbf{x}_1), \tag{2}$$

where $R_{pp}(\mathbf{x}_1,\mathbf{x}_1') = \overline{p(\mathbf{x}_1,t)p(\mathbf{x}_1',t)}$ is the time averaged two-point spatial correlation tensor. The eigenfunctions of this correlation tensor are mutually orthogonal by construction and they are usually chosen to be orthonormal:

$$\int_\Omega \phi^{(n)}(\mathbf{x}_1)\phi^{(m)}(\mathbf{x}_1)d\mathbf{x}_1 = \delta_{nm}, \tag{3}$$

with δ the Kronecker symbol. The projection of the pressure field (random function) onto $\phi^{(n)}$ gives the random projection coefficients, $a^{(n)}(t)$. Pressure field can be represented by a linear combination of deterministic mutually orthonormal modes weighted by these random coefficients:

$$p(\mathbf{x}_1,t) = \sum_n a^{(n)}(t)\phi^{(n)}(\mathbf{x}_1), \tag{4}$$

where $a^{(n)}(t) = \int_\Omega p(\mathbf{x}_1,t)\phi^{(n)}(\mathbf{x}_1)d\mathbf{x}_1$ are the random projection coefficients. The projection coefficients are mutually uncorrelated:

$$\overline{a^{(n)}(t)a^{(m)}(t)} = \delta_{nm}\lambda^{(n)}. \tag{5}$$

Considering the acoustic pressure defined in domain S, $p_{ac}(\mathbf{x}_2,t)$, extended modes are defined by [9, 20]:

$$\mathbf{x}_2 \in S \quad \psi^{(m)}(\mathbf{x}_2) = \frac{\overline{a^{(m)}(t)p_{ac}(\mathbf{x}_2,t)}}{\lambda^{(m)}}. \tag{6}$$

Based on this extended mode definition, Borée [9] proposed the following decomposition:

$$p_{ac}^C(\mathbf{x}_2,t) = \sum_n a^{(n)}(t)\psi^{(n)}(\mathbf{x}_2), \tag{7}$$

$$p_{ac}(\mathbf{x}_2,t) = p_{ac}^C(\mathbf{x}_2,t) + p_{ac}^D(\mathbf{x}_2,t), \tag{8}$$

where, quoting Borée [9]: p_{ac}^C *is the only part of signal* p_{ac} *correlated with* p. Note that if p_{ac} is completely uncorrelated to the pressure field in source region, one immediately has:

$$R_{p_{ac}p}(\mathbf{x}_1,\mathbf{x}_2) = \overline{p(\mathbf{x}_1,t)p_{ac}(\mathbf{x}_2,t)} = \sum_n \phi^{(n)}(\mathbf{x}_1)\overline{a^{(n)}(t)p_{ac}(\mathbf{x}_2,t)} = 0. \tag{9}$$

Hekmati *et al.* [21] propose to review this decomposition (equation (8)) for finite discrete domains. They discuss the absence of the uncorrelated part of the reconstructed acoustic pressure signal depending on: (i) the used POD formulation (classical or snapshot), (ii) the number of spatial points considered in source region, (iii) the available temporal samples. For finite discrete domains, two completely uncorrelated signals may mathematically exhibit a small correlation value which may not be associated with any physical correlation. This means that the equation (9) may not be satisfied for finite discrete domains even if p and p_{ac} are completely uncorrelated. Then, we propose to first define the threshold of the correlation operation for the given number of samples and to select only the extended modes for which the correlation value is higher than the defined threshold. For instance, suppose that we compute the correlation coefficient

$C(r,r')$ of two uncorrelated random signals: (r,r') of $N_t = 9334$ time-steps :

$$C(r,r') = \frac{1}{N_t}\sum_{i=1}^{N_t}\left(r(t_i)\times r'(t_i)\right) / \left(\sqrt{\overline{r}}\sqrt{\overline{r'}}\right). \qquad (10)$$

If the number of samples N_t was sufficient, one should have a $C(r,r')$ value of zero. The equation (10) is evaluated $N_{(r,r')} = 10^5$ times. Figure 5 represents the evolution of this coefficient for each realization. It is then observed that 99.9% of $C(r,r')$ values are inferior to a threshold of $\varepsilon = 0.034$. It means that when the coefficient correlation exhibits a value inferior to ε, the physical interpretation of this result may be questionable due to a problem of statistical convergence. Then, we propose to not to take into account the extended modes for which $C(a^{(n)}, p_{ac})$ is inferior to ε, the determined threshold.

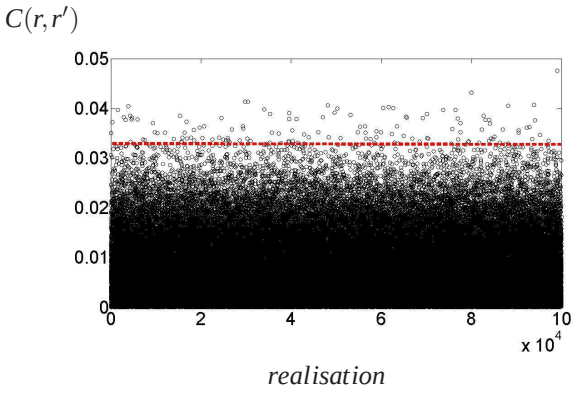

Figure 5. $C(r,r')$ correlation coefficient between two uncorrelated signals (r,r') of $N_t = 9334$ points each other. The dot line indicates the threshold ε that is 99.9% of the $N_{(r,r')}$ values of $C(r,r')$ are inferior to $\varepsilon = 0.034$.

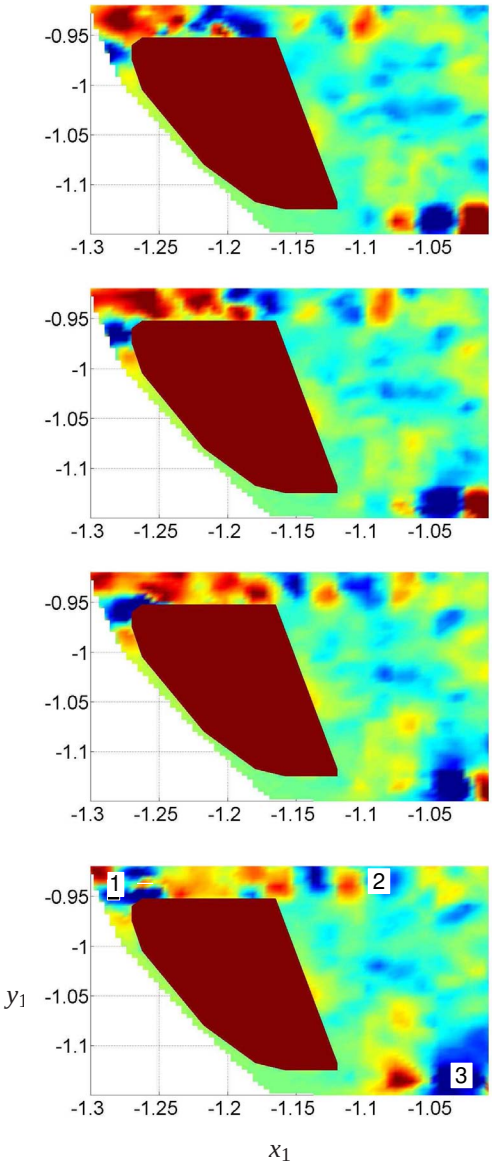

Figure 6. From top to bottom: successive instantaneous pressure field.

Results

Global results

Instantaneous pressure fields are presented in figure 6. The footprint of vortex sheddings can be visibly seen in the shear layer of two edges of the door mirror. Also one can notice the impact of turbulent structures generated by the A-pillar vortex on the inner edge of the door mirror.

The spectra of the pressure fluctuations for three indicated points in last image of figure 6 are calculated via the Welch method and represented by figure 7. A total number of 6 FFT blocks containing 3112 independent temporal samples with an overlap of 50% are averaged. A Hamming window is used. Each block represents 0.2 s of physical time. This procedure provides a frequency resolution of 4.8 Hz for the obtained spectra.

With respect to the frequency resolution, we can notice the emergence of a peak at 65 Hz for the point 1 located upstream the door mirror. Points 2 and 3 contain also a high level of energy around this frequency. The high level of the energy in this frequency may be related to the A-pillar vortex buffeting.

In point 3, the observed peak at 43 Hz can be related to the footprint of the vortex shedding of the door mirror with more sureness. Due to the 3D aspect of the flow the interpretation of observed peaks should be carried out with caution. However, by

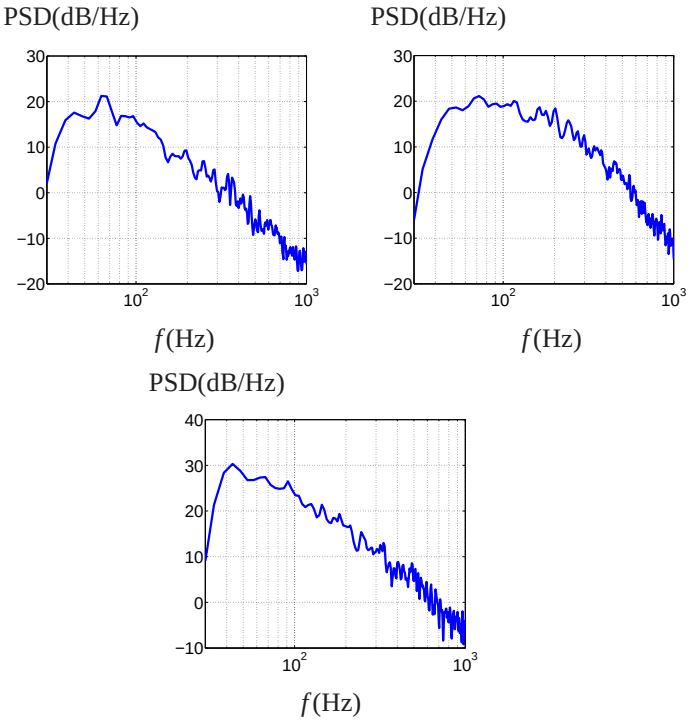

Figure 7. Power Spectral Density of the probed aerodynamic pressure field calculated by Welch method. Form left to right: corresponding PSD of points 1, 2 and 3 indicated in figure 6 respectively.

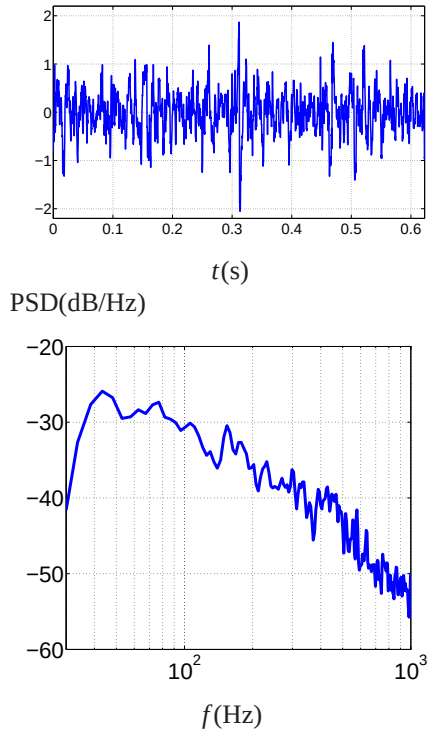

Figure 8. Acoustic pressure field probed in 0.55 m of the side window.Top: temporal signal. Bottom: corresponding PSD.

considering the mean flow velocity, $v_m = 33$ m/s, the y direction width of mirror in the selected zone (between the two mounting bases) $L = L_y = 0.16$ m and the observed frequency peak of the pressure spectrum of point 3 in 43 Hz, the Strouhal number $St = \frac{f.L}{v_m}$ equals to 0.21. This Strouhal number is quite close to the Strouhal number often observed in the wake of cylinder-like solids (Von Karman street).

As mentioned before the nearest point where the turbulent fluctuations are absent, is situated at 0.5 m of the left side of vehicle. The time signal and the corresponding Power Spectral Density (PSD) of the acoustic pressure in this point are presented in figure 8.

The acoustic pressure fluctuations spectrum in this region shows a peak around 75 Hz. At this frequency, point 2 (see figure 6) has a high level of energy. Also at 43 Hz, same as point 3 in the aerodynamic field, the acoustic field has a high level of energy. Based on these observations, as the acoustic pressure field and the aerodynamic one exhibit some similar frequency peaks, we use the EPOD in order to study the possibility of relating the acoustic pressure fluctuations to the aerodynamic events around the door mirror. In fact we expect that the peaks in the PSD of the pressure signal in the acoustic field should be related to the coherent turbulent activities in the source region. Then the use of POD may permit in the first step to identify the coherent structures in the source region and in the second step the EPOD may permit to study the relation between these structures and the generation of the acoustic pressure fluctuations.

POD

The application of the POD to aerodynamic pressure field provides a set of orthogonal modes. The modes are sorted according to their eigenvalue in a descendant order. The energy convergence of first 300 POD modes is represented in figure 9. The low energy content of the first modes shows the difficulty of extracting a global coherent feature of the flow in the considered measurement plan. This can be related to the nature of the 3D turbulent flow and also to the existence of two distinct regions of coherent structures related to vortex sheddings of inner and outer shear layers.

Figure 10 shows first modes of pressure field. One should notice that the energy related to each represented mode in figure 10 is contained in the associated eigenvalue and the colormap of spatial representation of modes (figure 10) does not contain any information about the energy. Two first POD modes act out partially the dynamic of outer shear layer of door mirror. Third and fifth modes represent mainly the inner wake. This separation confirms the recognition of two regions of coherent structures by

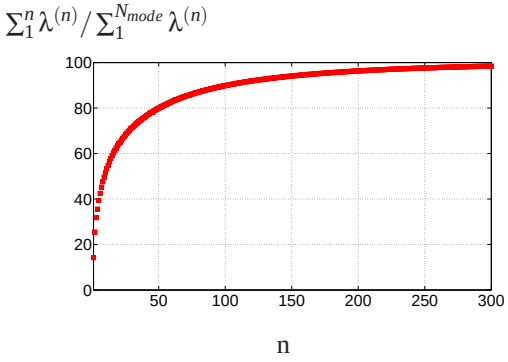

Figure 9. POD mode energy convergence, only the first 300 modes out of 1186 available ones are presented.

POD modes.

EPOD

According to equation (6) the extended modes are calculated by the use of the temporal projection coefficient of aerodynamic pressure field on the POD modes ($a^{(n)}(t)$) and the acoustic pressure signal (p_{ac}). As a first step all the extended modes are taken into account in order to reconstruct the acoustic pressure signal. Figure 11 shows the original acoustic pressure signal spectrum and the reconstructed one using all the extended modes. This application can somehow be compared to a direct correlation of the acoustic pressure field to the aerodynamic one in source region. The use of all POD modes (and necessarily all $a^{(n)}$) implies the full reconstruction of the aerodynamic pressure field in source region. As shown in figure 11 the acoustic pressure signal is mostly reconstructed when all the extended modes are considered. The use of all extended modes to reconstruct the acoustic pressure signal can be considered as studying the correlation of acoustic pressure signal and the whole pressure field in source region. However, such an application should be interpreted with extreme caution for finite discrete domains as the results may differ depending on the used POD formulation (snapshot or classic) and the spatial and temporal characteristics of the available data. For more details one can refer to Hekmati *et al.* [21].

As a second step only the extended modes associated with the most energetic POD modes in the Ω domain are selected. The last choice can be related to the conventional usage of the POD representing the coherent features of the flow. The followed idea consists in revealing the participation of the coherent structures of the flow in the generation of acoustic pressure fluctuations. For instance we have considered the extended modes related to the first 105 modes (representing 90% of the energy of the pressure field in domain Ω) in order to reconstruct the acoustic pressure signal. The PSD of the original pressure signal and the reconstructed one related to the first 105 modes are represented in figure 12. The PSD of the reconstructed signal and the

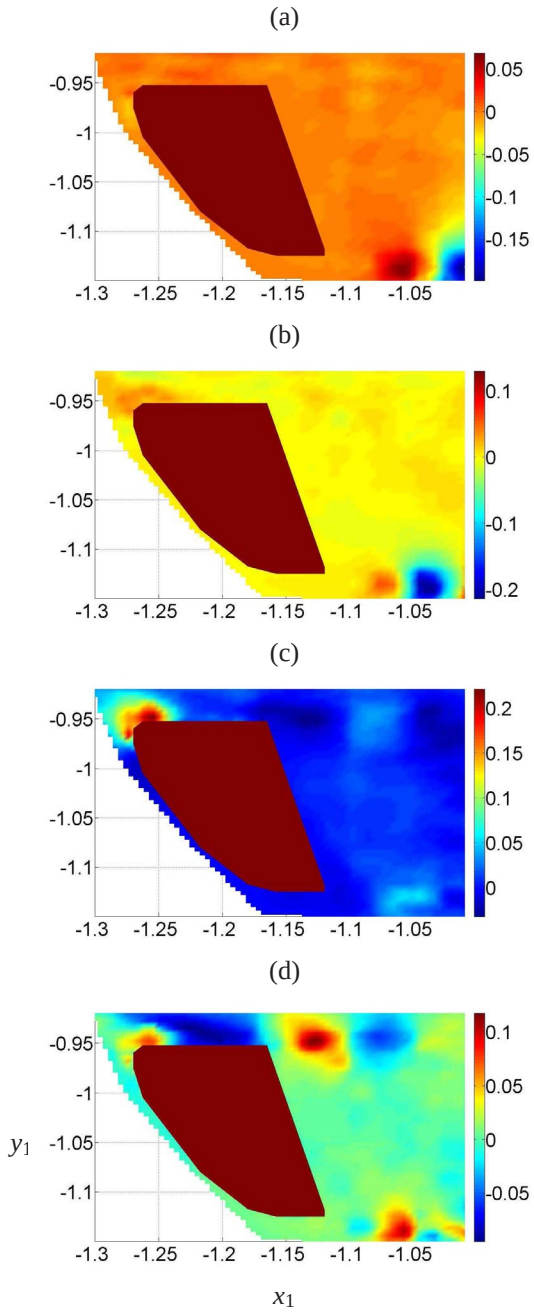

Figure 10. Spatial POD modes: (a)-(c) first, second and third modes, (d) fifth mode

PSD of the original pressure signal exhibits a similar shape up to 100 Hz. This reveals the participation of the coherent features of the aerodynamic field in the low frequency fluctuations of the acoustic pressure field.

As mentioned above, the last selection is related to conventional usage of POD in turbulent flows attempting to study the correlation between the coherent features and acoustic pressure.

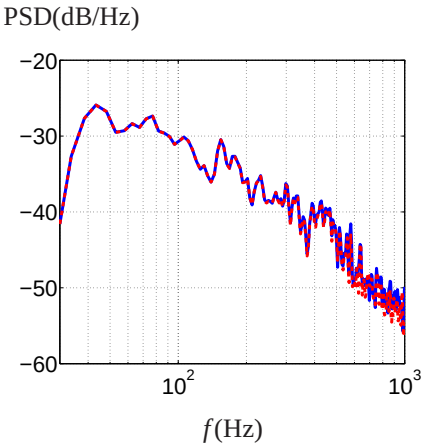

Figure 11. DSP of: (—)acoustic pressure signal, (– – –) acoustic pressure signal reconstructed by all available extended modes.

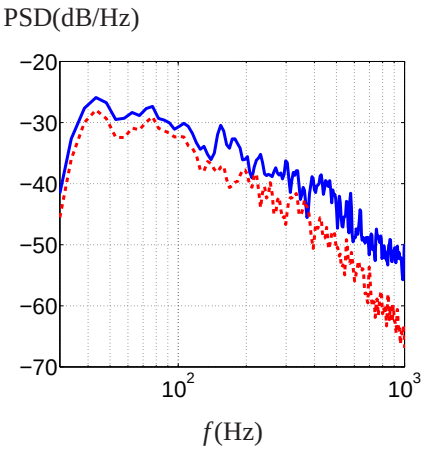

Figure 12. DSP of: (—)acoustic pressure signal, (– – –) acoustic pressure signal reconstructed by the extended modes associated with the first 105 most energetic modes representing 90% of pressure field's energy in source region.

The selection of POD modes can be done on any group of them that represent some selected dynamic features of the flow. But before any selection we need to insure the reliability of the extended modes from a statistical point of view. This verification is performed by the proposed procedure for threshold determination in *Followed methodology and mathematical tools* section.

Figure 13 displays the correlation coefficient between the temporal POD coefficients $a^{(n)}(t)$ and the acoustic pressure signal. On this figure the dot line indicates the threshold value from which the coefficient value can be investigated with 99.9% of confidence. It is then observed that only 177 modes out of 1186 ones available has a correlation coefficient higher than $\varepsilon = 0.034$. This then justifies the use of only these POD modes for such EPOD analysis. An analysis which uses the other Extended POD

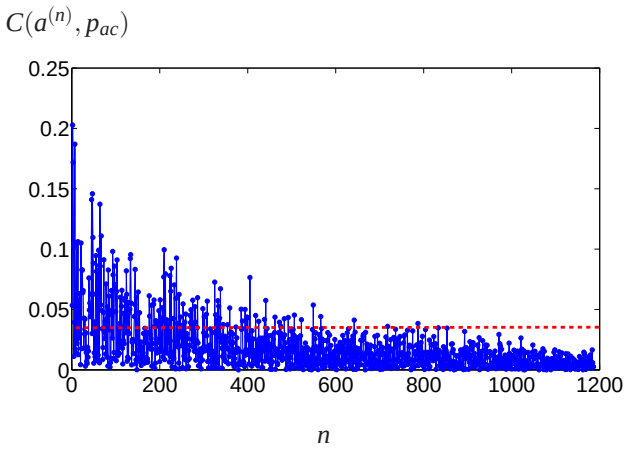

Figure 13. $C(a^{(n)}, p_{ac})$ correlation coefficient between the acoustic pressure signal and the temporal projection coefficient of aerodynamic pressure field on the POD modes in the source region.

modes may be erroneous due to a possible problem of statistical convergence. The POD modes corresponding to these converged extended modes contain 68.6% of the total energy of the aerodynamic pressure field in the source region. As one can observe on the figure 13 the converged EPOD modes are not necessarily related to the most energetic POD modes in source region.

The spectrum of acoustic pressure signal reconstructed by the converged EPOD modes is compared to the one of the original pressure signal on figure 14. Most of the frequency peaks are almost well represented by the converged extended modes. We can deduce that the most of the acoustic pressure fluctuations are surely related to the turbulent activities in the source region.

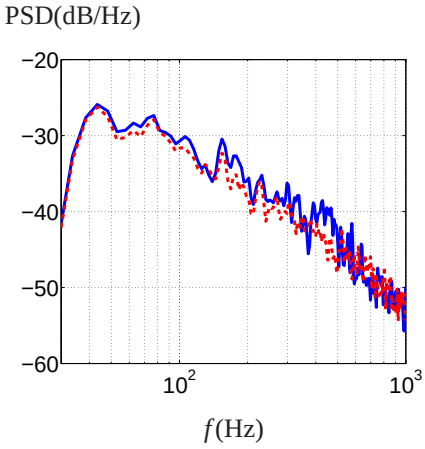

Figure 14. DSP of: (—) acoustic pressure signal, (– – –) acoustic pressure signal reconstructed by converged available extended modes.

It is then interesting to study the aerodynamic features that

the selected group of modes represents in the source region. For this purpose we propose to study the energy content of the pressure field in the source region. The energy is given by the RMS value at each spatial point of the pressure field regarding to equation (11).

$$p_{rms}(\mathbf{x}_1) = \sqrt{\overline{p(\mathbf{x}_1,t) \times p(\mathbf{x}_1,t)}} \qquad (11)$$

Figure 15 represents the energy of the aerodynamic pressure field reconstructed by the most energetic POD modes (the first 105 most energetic modes) and the one reconstructed by the POD modes corresponding to the converged EPOD modes. The aerodynamic pressure field reconstructed by the most energetic modes represents the dynamics of inner and the outer shear layers as well as the impact of the A-pillar vortex on the inner edge of the door mirror. The A-pillar vortex impact and especially, the inner shear layer are less present in the aerodynamic pressure field reconstructed by the POD modes corresponding to the converged EPOD modes. This observation (and considering figures 12 and 14) shows the high involvement of the outer shear layer in the generation of the acoustic pressure fluctuations for the most of the frequencies. Also, this signifies that for high frequencies the inner shear layer does not participate in the generation of the acoustic pressure fluctuations and it is physically decorrelated with the acoustic pressure measured at 0.55 m of the side window.

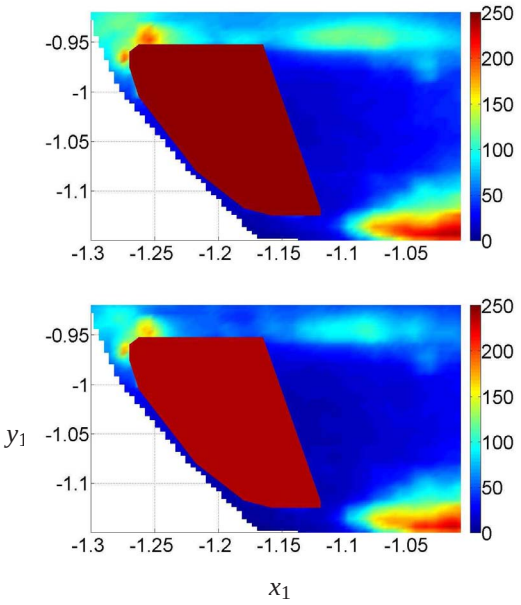

Figure 15. Energy content of the pressure field ($p_{rms}(\mathbf{x}_1)$). Top: reconstructed by the POD modes representing 90% of the total energy (first 105 modes). Bottom: reconstructed by the POD modes corresponding to the converged EPOD modes (representing 68.6% of the total energy).

Conclusion

A 3D Direct Noise Computation based on the Lattice Boltzmann methodology has been performed to investigate turbulent flow around an automobile vehicle. The numerical database has the advantage that the complete pressure field including the far-field acoustic pressure is entirely known. The aim of this study consists in investigating the contribution of the turbulent activities around the door mirror to the acoustic pressure fluctuations in its near neighborhood. The access to pressure field in source and acoustic far-field, makes possible to perform new applications of a post-processing mathematical tools aiming at revealing the correlation which exists between aerodynamic flow field and acoustic far-field. Thus, Extended Proper Orthogonal Decomposition procedure has been used for such investigation. Dealing with finite discrete domains, the convergence of the statistical operations should be examined when dealing with limited number of samples. A procedure is proposed in order to define a threshold to eliminate the non converged extended modes. The acoustic pressure is first estimated by the extended modes related to the most energetic POD modes representing 90% of energy of aerodynamic pressure field in the source region. The comparison of the acoustic pressure signal estimated by this selected modes and the original acoustic pressure signal shows a weak correlation level between the acoustic pressure field and the most coherent aerodynamic features. Then, the acoustic pressure is estimated using only the converged extended modes. The converged extended modes provide a better estimation of the acoustic pressure signal. This demonstrates the high correlation level between the acoustic pressure and the part of aerodynamic pressure that is represented by the POD modes corresponding to the selected extended modes. The reconstruction of the aerodynamic pressure field in source region by the POD modes corresponding to the converged EPOD modes reveals the high involvement of the outer shear layer in the generation of the acoustic pressure fluctuations.

Such analysis can then help to establish some strategies in order to control the flow features responsible of the sound emission with a better visibility.

REFERENCES

[1] Adam, J., Ricot, D., Dubief, C., and Guy, C., 2008. "Aeroacoustics simulation of automative ventilation outlets". *Proceedings Acoustics'08, Paris,France*, pp. 1863–1866.

[2] Adam, J., and Ricot, D., 2009. "Direct aeroacoustic source identification based on lattice boltzmann simulation and beamforming technique". *AIAA Paper 2009-1382*.

[3] Bogey, C., and Bailly, C., 2007. "An analysis of the corre-

lations between the turbulent flow and the sound pressure fields of subsonic jets". *J. Fluid Mech.,* ***583***, pp. 71–91.

[4] Druault, P., Yu, M., and Sagaut, P., 2010. "Quadratic stochastic estimation of far field acoustic pressure with coherent structure events in a 2d compressible plane mixing layer". *Int. J. Numer. Meth. Fluids,* ***62***, pp. 906–926.

[5] Jordan, P., and Gervais, Y., 2008. "Subsonic jet aeroacoustics: associating experiment, modelling and simulation". *Exp. Fluids,* ***44***(1), pp. 1–21.

[6] Panda, J., Seasholtz, R., and Elam, K., 2005. "Investigation of noise sources in high-speed jets via correlation measurements". *J. Fluid Mech.,* ***537***, pp. 349–385.

[7] Freund, J., 2001. "Noise sources in a low-reynolds-number turbulent jet at mach 0.9". *J. Fluid Mech.,* ***438***, pp. 277–305.

[8] Lighthill, M., 1952. "On sound generated aerodynamically: I. general theory". *Proc. R. Soc. London,* ***211***, pp. 564–587.

[9] Borée, J., 2003. "Extended proper orthogonal decomposition: a tool to analyse correlated events in turbulent flows". *Exp. Fluids,* ***35***, pp. 188–192.

[10] Chen, S., and Doolen, G., 1998. "Lattice boltzmann method for fluid flows". *Annu. Rev. Fluid Mech,* ***30***, pp. 329–364.

[11] Ricot, D., Maillard, V., and Bailly, C., 2002. "Numerical simulation of unsteady cavity flow using lattice boltzmann method". *AIAA Paper 2002-2532*.

[12] Marié, S., Ricot, D., and Sagaut, P., 2007. "Accuracy of lattice boltzmann method for aeroacoustics simulations". *AIAA paper 2007-3515*.

[13] Marié, S., Ricot, D., and Sagaut, P., 2009. "Comparison between lattice boltzmann method and navierstokes high order schemes for computational aeroacoustics". *J. Comput. Phys.,* ***228***, pp. 1056–1070.

[14] Skordos, P., 1995. "Modeling flue organ pipes: subsonic flow, lattice boltzmann, and parallel distributed computers". PhD Thesis, Massachusetts Institute of Technology.

[15] Buick, J., Greated, C., and Campbell, D., 1998. "Lattice bgk simulation of sound waves". *Europhys. Lett.,* ***43***(3), pp. 235–240.

[16] Wilde, A., 2004. "Flow acoustic simulations using the lattice-boltzmann method". *Proceedings of 22nd CAD-FEM Users Meeting, Int. Congress on FEM Technolog with ANSYS CFX & ICEM CFD Conference, Dresden, Germany*.

[17] B.Crouse, Freed, D., Balasubramanian, G., Senthooran, S., Lew, P., and Mongeau, L., 2006. "Fundamental aeroacoustic capabilities of the lattice-boltzmann method". *AIAA paper 2006-2571*.

[18] Lumley, J., 1967. *The structure of inhomogeneous turbulent flows*. Yaglom and Tatarsky eds.

[19] Holmes, P., Lumley, J., and Berkooz, G., 1996. *Turbulence, coherent structures, dynamical systems and symmetry*. Cambridge Monograph on Mechanics ed.

[20] Maurel, S., Boree, J., and Lumley, J., 2001. "Extended proper orthogonal decomposition: application to jet/vortex interaction". *Flow Turbulence Combust,* ***67***, pp. 125–136.

[21] Hekmati, A., D.Ricot, and Druault, P. "Extended proper orthogonal decomposition: A tool for aeroacoustic analysis". *submitted to: Int. Journal of Aeroacoustic*.